

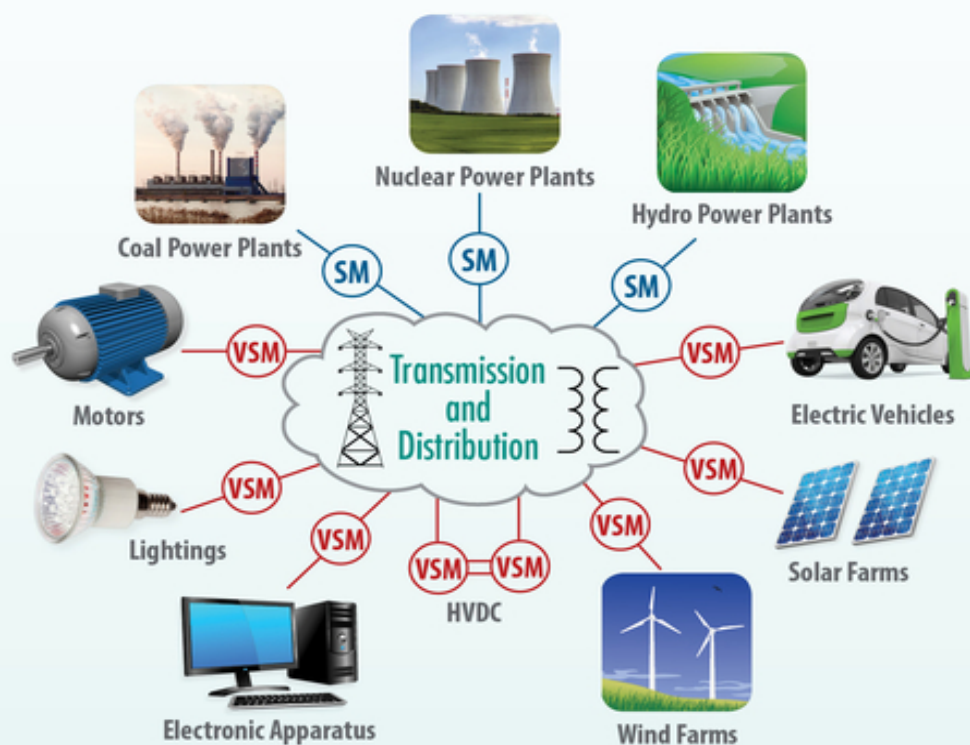
---

# Power Electronics-Enabled Autonomous Power Systems

## Next Generation Smart Grids

---

**Qing-Chang Zhong**





## **Power Electronics-Enabled Autonomous Power Systems**



# **Power Electronics-Enabled Autonomous Power Systems**

Next Generation Smart Grids

*Qing-Chang Zhong*

Illinois Institute of Technology & Syndem LLC  
Chicago, USA

**WILEY**

  
**IEEE PRESS**

This edition first published 2020  
© 2020 John Wiley & Sons Ltd

All rights reserved. No part of this publication may be reproduced, stored in a retrieval system, or transmitted, in any form or by any means, electronic, mechanical, photocopying, recording or otherwise, except as permitted by law. Advice on how to obtain permission to reuse material from this title is available at <http://www.wiley.com/go/permissions>.

The right of Qing-Chang Zhong to be identified as the author of this work has been asserted in accordance with law.

#### *Registered Offices*

John Wiley & Sons, Inc., 111 River Street, Hoboken, NJ 07030, USA  
John Wiley & Sons Ltd, The Atrium, Southern Gate, Chichester, West Sussex, PO19 8SQ, UK

#### *Editorial Office*

The Atrium, Southern Gate, Chichester, West Sussex, PO19 8SQ, UK

For details of our global editorial offices, customer services, and more information about Wiley products visit us at [www.wiley.com](http://www.wiley.com).

Wiley also publishes its books in a variety of electronic formats and by print-on-demand. Some content that appears in standard print versions of this book may not be available in other formats.

#### *Limit of Liability/Disclaimer of Warranty*

MATLAB<sup>®</sup> is a trademark of The MathWorks, Inc. and is used with permission. The MathWorks does not warrant the accuracy of the text or exercises in this book. This work's use or discussion of MATLAB<sup>®</sup> software or related products does not constitute endorsement or sponsorship by The MathWorks of a particular pedagogical approach or particular use of the MATLAB<sup>®</sup> software. In view of ongoing research, equipment modifications, changes in governmental regulations, and the constant flow of information relating to the use of experimental reagents, equipment, and devices, the reader is urged to review and evaluate the information provided in the package insert or instructions for each chemical, piece of equipment, reagent, or device for, among other things, any changes in the instructions or indication of usage and for added warnings and precautions. While the publisher and author have used their best efforts in preparing this work, they make no representations or warranties with respect to the accuracy or completeness of the contents of this work and specifically disclaim all warranties, including without limitation any implied warranties of merchantability or fitness for a particular purpose. No warranty may be created or extended by sales representatives, written sales materials or promotional statements for this work. The fact that an organization, website, or product is referred to in this work as a citation and/or potential source of further information does not mean that the publisher and author endorse the information or services the organization, website, or product may provide or recommendations it may make. This work is sold with the understanding that the publisher is not engaged in rendering professional services. The advice and strategies contained herein may not be suitable for your situation. You should consult with a specialist where appropriate. Further, readers should be aware that websites listed in this work may have changed or disappeared between when this work was written and when it is read. Neither the publisher nor author shall be liable for any loss of profit or any other commercial damages, including but not limited to special, incidental, consequential, or other damages.

#### *Library of Congress Cataloging-in-Publication data applied for*

HB ISBN: 9781118803523

Cover Design: Wiley

Cover Images: Electric Car © Nerthuz/Getty Images, Computer Technology © RoyFWylam/Getty Images, Led light bulb © ppart/Shutterstock, Industrial electric motor © scanrail/Getty Images, Hydro dam water © ChrisGorgio/Getty Images, Solar Panel © filo/Getty Images, Energy © Voyagerix/Shutterstock, Nuclear power plant © TTstudio/Shutterstock, A field of wind turbines © linearcures/Getty Images

Set in 9.5/12.5pt STIXTwoText by SPi Global, Chennai, India

Printed and bound by CPI Group (UK) Ltd, Croydon, CR0 4YY

To

*Ms. Lihua Luo, my first-grade teacher, who told me:*

*“you have nothing but potential. Keep moving forward. Never stop.”*

*and*

*Ms. Xiufen Lin, my third-grade teacher, who told me:*

*“you have nothing but do not envy others.”*



## Contents

<b>List of Figures</b>	<i>xix</i>
<b>List of Tables</b>	<i>xxxiii</i>
<b>Foreword</b>	<i>xxxv</i>
<b>Preface</b>	<i>xxxvii</i>
<b>Acknowledgments</b>	<i>xxxix</i>
<b>About the Author</b>	<i>xli</i>
<b>List of Abbreviations</b>	<i>xliii</i>
<b>1</b>	<b>Introduction</b> <i>1</i>
1.1	Motivation and Purpose <i>1</i>
1.2	Outline of the Book <i>3</i>
1.3	Evolution of Power Systems <i>7</i>
1.3.1	Today's Grids <i>8</i>
1.3.2	Smart Grids <i>8</i>
1.3.3	Next-Generation Smart Grids <i>8</i>
1.4	Summary <i>10</i>
	<b>Part I Theoretical Framework</b> <i>11</i>
<b>2</b>	<b>Synchronized and Democratized (SYNDEM) Smart Grid</b> <i>13</i>
2.1	The SYNDEM Concept <i>13</i>
2.2	SYNDEM Rule of Law – Synchronization Mechanism of Synchronous Machines <i>15</i>
2.3	SYNDEM Legal Equality – Homogenizing Heterogeneous Players as Virtual Synchronous Machines (VSM) <i>18</i>
2.4	SYNDEM Grid Architecture <i>19</i>
2.4.1	Architecture of Electrical Systems <i>19</i>
2.4.2	Overall Architecture <i>22</i>
2.4.3	Typical Scenarios <i>23</i>
2.4.3.1	Home Grid <i>23</i>
2.4.3.2	Neighborhood Grid <i>23</i>

2.4.3.3	Community Grid	23
2.4.3.4	District Grid	24
2.4.3.5	Regional Grid	24
2.5	Potential Benefits	24
2.6	Brief Description of Technical Routes	28
2.6.1	The First-Generation (1G) VSM	28
2.6.2	The Second-Generation (2G) VSM	29
2.6.3	The Third-Generation (3G) VSM	29
2.7	Primary Frequency Response (PFR) in a SYNDEM Smart Grid	30
2.7.1	PFR from both Generators and Loads	31
2.7.2	Droop	31
2.7.3	Fast Action Without Delay	31
2.7.4	Reconfigurable Virtual Inertia	31
2.7.5	Continuous PFR	32
2.8	SYNDEM Roots	32
2.8.1	SYNDEM and Taoism	32
2.8.2	SYNDEM and Chinese History	33
2.9	Summary	34

### **3 Ghost Power Theory 35**

3.1	Introduction	35
3.2	Ghost Operator, Ghost Signal, and Ghost System	36
3.2.1	The Ghost Operator	36
3.2.2	The Ghost Signal	37
3.2.3	The Ghost System	39
3.3	Physical Meaning of Reactive Power in Electrical Systems	41
3.4	Extension to Complete the Electrical-Mechanical Analogy	43
3.5	Generalization to Other Energy Systems	46
3.6	Summary and Discussions	47

## **Part II 1G VSM: Synchronverters 49**

### **4 Synchronverter Based Generation 51**

4.1	Mathematical Model of Synchronous Generatorss	51
4.1.1	The Electrical Part	51
4.1.2	The Mechanical Part	53
4.1.3	Presence of a Neutral Line	54
4.2	Implementation of a Synchronverter	55
4.2.1	The Power Part	56
4.2.2	The Electronic Part	56
4.3	Operation of a Synchronverter	57
4.3.1	Regulation of Real Power and Frequency Droop Control	57
4.3.2	Regulation of Reactive Power and Voltage Droop Control	58
4.4	Simulation Results	59

4.4.1	Under Different Grid Frequencies	60
4.4.2	Under Different Load Conditions	62
4.5	Experimental Results	62
4.5.1	Grid-connected Set Mode	63
4.5.2	Grid-connected Droop Mode	63
4.5.3	Grid-connected Parallel Operation	63
4.5.4	Seamless Transfer of the Operation Mode	64
4.6	Summary	67
<b>5</b>	<b>Synchronverter Based Loads</b>	<b>69</b>
5.1	Introduction	69
5.2	Modeling of a Synchronous Motor	70
5.3	Operation of a PWM Rectifier as a VSM	71
5.3.1	Controlling the Power	72
5.3.2	Controlling the DC-bus Voltage	73
5.4	Simulation Results	74
5.4.1	Controlling the Power	74
5.4.2	Controlling the DC-bus Voltage	76
5.5	Experimental Results	77
5.5.1	Controlling the Power	77
5.5.2	Controlling the DC-bus Voltage	77
5.6	Summary	79
<b>6</b>	<b>Control of Permanent Magnet Synchronous Generator (PMSG) Based Wind Turbines</b>	<b>81</b>
6.1	Introduction	81
6.2	PMSG Based Wind Turbines	83
6.3	Control of the Rotor-Side Converter	83
6.4	Control of the Grid-Side Converter	85
6.5	Real-time Simulation Results	86
6.5.1	Under Normal Grid Conditions	87
6.5.1.1	GSC Performance	88
6.5.1.2	RSC Performance	88
6.5.2	Under Grid Faults	89
6.6	Summary	90
<b>7</b>	<b>Synchronverter Based AC Ward Leonard Drive Systems</b>	<b>91</b>
7.1	Introduction	91
7.2	Ward Leonard Drive Systems	93
7.3	Model of a Synchronous Generator	95
7.4	Control Scheme with a Speed Sensor	96
7.4.1	Control Structure	96
7.4.2	System Analysis and Parameter Selection	97
7.5	Control Scheme without a Speed Sensor	98
7.5.1	Control Structure	98

7.5.2	System Analysis and Parameter Selection	99
7.6	Experimental Results	100
7.6.1	Case 1: With a Speed Sensor for Feedback	101
7.6.1.1	Reversal from a High Speed without a Load	101
7.6.1.2	Reversal from a High Speed with a Load	101
7.6.1.3	Reversal from a Low Speed without a Load	102
7.6.1.4	Reversal from a Low Speed with a Load	102
7.6.1.5	Reversal at an Extremely Low Speed without a Load	102
7.6.2	Case 2: Without a Speed Sensor for Feedback	104
7.6.2.1	Reversal from a High Speed without a Load	104
7.6.2.2	Reversal from a High Speed with a Load	104
7.7	Summary	106
<b>8</b>	<b>Synchronverter without a Dedicated Synchronization Unit</b>	<b>107</b>
8.1	Introduction	107
8.2	Interaction of a Synchronous Generator (SG) with an Infinite Bus	109
8.3	Controller for a Self-synchronized Synchronverter	110
8.3.1	Operation after Connection to the Grid	112
8.3.2	Synchronization before Connection to the Grid	113
8.4	Simulation Results	114
8.4.1	Normal Operation	114
8.4.2	Operation under Grid Faults	118
8.5	Experimental Results	119
8.5.1	Case 1: With the Grid Frequency Below 50 Hz	119
8.5.2	Case 2: With the Grid Frequency Above 50 Hz	123
8.6	Benefits of Removing the Synchronization Unit	123
8.7	Summary	124
<b>9</b>	<b>Synchronverter Based Loads without a Dedicated Synchronisation Unit</b>	<b>125</b>
9.1	Controlling the DC-bus Voltage	125
9.1.1	Self-synchronization	125
9.1.2	Normal Operation	126
9.2	Controlling the Power	127
9.3	Simulation Results	127
9.3.1	Controlling the DC-bus Voltage	128
9.3.2	Controlling the Power	130
9.4	Experimental Results	131
9.4.1	Controlling the DC-bus Voltage	132
9.4.2	Controlling the Power	132
9.5	Summary	134
<b>10</b>	<b>Control of a DFIG Based Wind Turbine as a VSG (DFIG-VSG)</b>	<b>135</b>
10.1	Introduction	135
10.2	DFIG Based Wind Turbines	137

10.3	Differential Gears and Ancient Chinese South-pointing Chariots	138
10.4	Analogy between a DFIG and Differential Gears	139
10.5	Control of a Grid-side Converter	140
10.5.1	DC-bus Voltage Control	141
10.5.2	Unity Power Factor Control	141
10.5.3	Self-synchronization	142
10.6	Control of the Rotor-Side Converter	142
10.6.1	Frequency Control	143
10.6.2	Voltage Control	143
10.6.3	Self-synchronization	144
10.7	Regulation of System Frequency and Voltage	145
10.8	Simulation Results	146
10.9	Experimental Results	150
10.10	Summary	153
<b>11</b>	<b>Synchronverter Based Transformerless Photovoltaic Systems</b>	<b>155</b>
11.1	Introduction	155
11.2	Leakage Currents and Grounding of Grid-tied Converters	156
11.2.1	Ground, Grounding, and Grounded Systems	156
11.2.2	Leakage Currents in a Grid-tied Converter	158
11.2.3	Benefits of Providing a Common AC and DC Ground	159
11.3	Operation of a Conventional Half-bridge Inverter	160
11.3.1	Reduction of Leakage Currents	161
11.3.2	Output Voltage Range	161
11.4	A Transformerless PV Inverter	161
11.4.1	Topology	161
11.4.2	Control of the Neutral Leg	161
11.4.3	Control of the Inversion Leg as a VSM	164
11.4.3.1	Real Power Control and Frequency Droop	164
11.4.3.2	Reactive Power Control and Voltage Droop	165
11.4.3.3	Synchronization	165
11.5	Real-time Simulation Results	165
11.6	Summary	167
<b>12</b>	<b>Synchronverter Based STATCOM without an Dedicated Synchronization Unit</b>	<b>169</b>
12.1	Introduction	169
12.2	Conventional Control of STATCOM	170
12.2.1	Operational Principles	171
12.2.2	Typical Control Strategy	172
12.3	Synchronverter Based Control	173
12.3.1	Regulation of the DC-bus Voltage and Synchronization with the Grid	173
12.3.2	Operation in the Q-mode to Regulate the Reactive Power	175
12.3.3	Operation in the V-mode to Regulate the PCC Voltage	176
12.3.4	Operation in the $V_D$ -mode to Droop the Voltage	176

12.4	Simulation Results	177
12.4.1	System Description	177
12.4.2	Connection to the Grid	179
12.4.3	Normal Operation in Different Modes	180
12.4.4	Operation under Extreme Conditions	181
12.4.4.1	With a Changing Grid Frequency	181
12.4.4.2	With a Changing Grid Voltage	183
12.4.4.3	With a Changing System Strength	184
12.5	Summary	185
<b>13</b>	<b>Synchronverters with Bounded Frequency and Voltage</b>	<b>187</b>
13.1	Introduction	187
13.2	Model of the Original Synchronverter	188
13.3	Achieving Bounded Frequency and Voltage	189
13.3.1	Control Design	190
13.3.1.1	Maintaining the Frequency within a Given Range	190
13.3.1.2	Maintaining the Voltage within a Given Range	191
13.3.2	Existence of a Unique Equilibrium	193
13.3.2.1	Theoretical Analysis	193
13.3.2.2	A Numerical Example	195
13.3.3	Convergence to the Equilibrium	197
13.3.3.1	Stability of the Fast Dynamics	197
13.3.3.2	Stability of the Slow Dynamics	197
13.4	Real-time Simulation Results	199
13.5	Summary	202
<b>14</b>	<b>Virtual Inertia, Virtual Damping, and Fault Ride-through</b>	<b>203</b>
14.1	Introduction	203
14.2	Inertia, the Inertia Time Constant, and the Inertia Constant	204
14.3	Limitation of the Inertia of a Synchronverter	206
14.4	Reconfiguration of the Inertia Time Constant	210
14.4.1	Design and Outcome	210
14.4.2	What is the Catch?	211
14.5	Reconfiguration of the Virtual Damping	212
14.5.1	Through Impedance Scaling with an Inner-loop Voltage Controller	213
14.5.1.1	Controller Design and Analysis	213
14.5.1.2	Enhancement of Voltage Quality	213
14.5.2	Through Impedance Insertion with an Inner-loop Current Controller	214
14.6	Fault Ride-through	214
14.6.1	Analysis	214
14.6.2	Recommended Design	215
14.7	Simulation Results	215
14.7.1	A Single VSM	216
14.7.1.1	Reconfigurability of Virtual Inertia and Virtual Damping	216
14.7.1.2	Effect of the Virtual Damping	216

14.7.2	Two VSMs in Parallel Operation	217
14.7.2.1	Case 1: $J_{v1} = J_{v2} = 1 \text{ s}$	218
14.7.2.2	Case 2: $J_{v1} \neq J_{v2}$	218
14.7.2.3	Fault Ride-through	219
14.8	Experimental Results	221
14.8.1	A Single VSM	221
14.8.1.1	Reconfigurability of the Inertia Time Constant and Damping	221
14.8.1.2	Effect of the Virtual Damping	221
14.8.2	Two VSMs in Parallel Operation	222
14.9	Summary	225

### Part III 2G VSM: Robust Droop Controller 227

<b>15</b>	<b>Synchronization Mechanism of Droop Control</b>	<b>229</b>
15.1	Brief Review of Phase-Locked Loops (PLLs)	229
15.1.1	Basic PLL	229
15.1.2	Enhanced PLL (EPLL)	230
15.2	Brief Review of Droop Control	232
15.3	Structural Resemblance between Droop Control and PLL	234
15.3.1	When the Impedance is Inductive	234
15.3.2	When the Impedance is Resistive	236
15.4	Operation of a Droop Controller as a Synchronization Unit	238
15.5	Experimental Results	239
15.5.1	Synchronization with the Grid	239
15.5.2	Connection to the Grid	240
15.5.3	Operation in the Droop Mode	241
15.5.4	Robustness of Synchronization	241
15.5.5	Change in the Operation Mode	242
15.6	Summary	243
<b>16</b>	<b>Robust Droop Control</b>	<b>245</b>
16.1	Control of Inverter Output Impedance	245
16.1.1	Inverters with Inductive Output Impedances (L-inverters)	245
16.1.2	Inverters with Resistive Output Impedances (R-inverters)	246
16.1.3	Inverters with Capacitive Output Impedances (C-inverters)	247
16.2	Inherent Limitations of Conventional Droop Control	248
16.2.1	Basic Principle	248
16.2.2	Experimental Phenomena	250
16.2.3	Real Power Sharing	251
16.2.4	Reactive Power Sharing	252
16.3	Robust Droop Control of R-inverters	252
16.3.1	Control Strategy	252
16.3.2	Error due to Inaccurate Voltage Measurements	253
16.3.3	Voltage Regulation	254

16.3.4	Error due to the Global Settings for $E^*$ and $\omega^*$	254
16.3.5	Experimental Results	255
16.3.5.1	Inverters having Different Per-unit Output Impedances with a Linear Load	255
16.3.5.2	Inverters having the Same Per-unit Output Impedance with a Linear Load	257
16.3.5.3	With a Nonlinear Load	257
16.4	Robust Droop Control of C-inverters	261
16.4.1	Control Strategy	261
16.4.2	Experimental Results	262
16.4.2.1	With a Linear Load	262
16.4.2.2	With a Nonlinear Load	262
16.5	Robust Droop Control of L-inverters	262
16.5.1	Control Strategy	262
16.5.2	Experimental Results	265
16.5.2.1	With a Linear Load	268
16.5.2.2	With a Nonlinear Load	268
16.6	Summary	268
<b>17</b>	<b>Universal Droop Control</b>	<b>269</b>
17.1	Introduction	269
17.2	Further Insights into Droop Control	270
17.2.1	Parallel Operation of Inverters with the Same Type of Impedance	271
17.2.2	Parallel Operation of L-, R-, and $R_L$ -inverters	272
17.2.3	Parallel Operation of $R_C$ -, R-, and C-inverters	273
17.3	Universal Droop Controller	275
17.3.1	Basic Principle	275
17.3.2	Implementation	276
17.4	Real-time Simulation Results	277
17.5	Experimental Results	277
17.5.1	Case I: Parallel Operation of L- and C-inverters	277
17.5.2	Case II: Parallel Operation of L-, C-, and R-inverters	279
17.6	Summary	281
<b>18</b>	<b>Self-synchronized Universal Droop Controller</b>	<b>283</b>
18.1	Description of the Controller	283
18.2	Operation of the Controller	285
18.2.1	Self-synchronization Mode	285
18.2.2	Set Mode ( $P$ -mode and $Q$ -mode)	286
18.2.3	Droop Mode ( $P_D$ -mode and $Q_D$ -mode)	286
18.3	Experimental Results	287
18.3.1	R-inverter with Self-synchronized Universal Droop Control	288
18.3.1.1	Self-synchronization	288
18.3.1.2	Connection to the Grid	288
18.3.1.3	Regulation of Real and Reactive Power	289
18.3.1.4	Impact of Change in the DC-bus Voltage $V_{DC}$	290
18.3.2	L-inverter with Self-synchronized Universal Droop Control	290

18.3.2.1	Self-synchronization	290
18.3.2.2	Connection to the Grid	290
18.3.2.3	Regulation of Real and Reactive Power	291
18.3.2.4	Impact of the Change in the DC-bus Voltage	293
18.3.3	L-inverter with Self-synchronized Robust Droop Control	294
18.3.3.1	Self-synchronization	295
18.3.3.2	Connection to the Grid	295
18.3.3.3	Regulation of Real and Reactive Power	295
18.3.3.4	Impact of the Change in the DC-bus Voltage	296
18.4	Real-time Simulation Results from a Microgrid	297
18.5	Summary	300
<b>19</b>	<b>Droop-Controlled Loads for Continuous Demand Response</b>	<b>301</b>
19.1	Introduction	301
19.2	Control Framework with a Three-port Converter	302
19.2.1	Generation of the Real Power Reference	302
19.2.2	Regulation of the Power Drawn from the Grid	304
19.2.3	Analysis of the Operation Modes	305
19.2.4	Determination of the Capacitance for Grid Support	306
19.3	An Illustrative Implementation with the $\theta$ -converter	308
19.3.1	Brief Description about the $\theta$ -converter	309
19.3.2	Control of the Neutral Leg	310
19.3.3	Control of the Conversion Leg	311
19.4	Experimental Results	311
19.4.1	Design of the Experimental System	311
19.4.2	Steady-state Performance	312
19.4.2.1	Operation under the Grid-support Mode	312
19.4.2.2	Operation under the No-support Mode	314
19.4.3	Transient Performance	315
19.4.3.1	System Start-up	315
19.4.3.2	Connection of the Load	316
19.4.4	Capacity Potential	317
19.4.5	Comparative Study	318
19.5	Summary	319
<b>20</b>	<b>Current-limiting Universal Droop Controller</b>	<b>321</b>
20.1	Introduction	321
20.2	System Modeling	322
20.3	Control Design	323
20.3.1	Structure	323
20.3.2	Implementation	323
20.4	System Analysis	326
20.4.1	Current-limiting Property	326
20.4.2	Closed-loop Stability	327
20.4.3	Selection of Control Parameters	328

20.5	Practical Implementation	329
20.6	Operation under Grid Variations and Faults	330
20.7	Experimental Results	331
20.7.1	Operation under Normal Conditions	332
20.7.2	Operation under Grid Faults	334
20.8	Summary	338

## Part IV 3G VSM: Cybersync Machines 339

<b>21</b>	<b>Cybersync Machines</b>	<b>341</b>
21.1	Introduction	341
21.2	Passivity and Port-Hamiltonian Systems	343
21.2.1	Passive Systems	343
21.2.2	Port-Hamiltonian Systems	343
21.2.3	Passivity of Interconnected Passive Systems	345
21.3	System Modeling	346
21.4	Control Framework	348
21.4.1	The Engendering Block $\Sigma_e$	349
21.4.2	Generation of the Desired Frequency $\omega_d$ and Flux $\varphi_d$	350
21.4.3	Design of $\Sigma_\omega$ and $\Sigma_\varphi$ to Obtain a Passive $\Sigma_C$	351
21.5	Passivity of the Controller	352
21.5.1	Losslessness of the Interconnection Block $\Sigma_I$	352
21.5.2	Passivity of the Cascade of $\Sigma_C$ and $\Sigma_I$	354
21.6	Passivity of the Closed-loop System	355
21.7	Sample Implementations for Blocks $\Sigma_\omega$ and $\Sigma_\varphi$	355
21.7.1	Using the Standard Integral Controller (IC)	355
21.7.2	Using a Static Controller	356
21.8	Self-Synchronization and Power Regulation	357
21.9	Simulation Results	358
21.9.1	Self-synchronization	360
21.9.2	Operation after Connection to the Grid	360
21.10	Experimental Results	362
21.10.1	Self-synchronization	362
21.10.2	Operation after Connection to the Grid	363
21.11	Summary	364

## Part V Case Studies 365

<b>22</b>	<b>A Single-node System</b>	<b>367</b>
22.1	SYNDEM Smart Grid Research and Educational Kit	367
22.1.1	Overview	367
22.1.2	Hardware Structure	368
22.1.2.1	Power Board	368

22.1.2.2	Control Board	369
22.1.3	Sample Conversion Topologies Attainable	369
22.1.3.1	DC–DC Converters	370
22.1.3.2	Uncontrolled Rectifiers	370
22.1.3.3	PWM-controlled Rectifiers	371
22.1.3.4	$\theta$ -Converters	372
22.1.3.5	Inverters	372
22.1.3.6	DC–DC–AC Converters	373
22.1.3.7	Single-phase AC–DC–AC Back-to-Back Converters	373
22.1.3.8	Three-phase AC–DC–AC Back-to-Back Converters	373
22.2	Details of the Single-Node SYNDEM System	375
22.2.1	Description of the System	375
22.2.2	Experimental Results	377
22.3	Summary	378
<b>23</b>	<b>A 100% Power Electronics Based SYNDEM Smart Grid Testbed</b>	<b>379</b>
23.1	Description of the Testbed	379
23.1.1	Overall Structure	379
23.1.2	VSM Topologies Adopted	379
23.1.2.1	$\theta$ -Converter	380
23.1.2.2	Beijing Converter	381
23.1.3	Individual Nodes	382
23.1.3.1	Energy Bridges	382
23.1.3.2	Solar Power Nodes	383
23.1.3.3	Wind Power Nodes	383
23.1.3.4	DC-Load Node	383
23.1.3.5	AC-Load Node	383
23.2	Experimental Results	384
23.2.1	Operation of Energy Bridges	384
23.2.2	Operation of Solar Power Nodes	384
23.2.3	Operation of Wind Power Nodes	386
23.2.4	Operation of the DC-Load Node	388
23.2.5	Operation of the AC-Load Node	389
23.2.6	Operation of the Whole Testbed	391
23.3	Summary	393
<b>24</b>	<b>A Home Grid</b>	<b>395</b>
24.1	Description of the Home Grid	395
24.2	Results from Field Operations	396
24.2.1	Black start and Grid forming	396
24.2.2	From Islanded to Grid-tied Operation	399
24.2.3	Seamless Mode Change when the Public Grid is Lost and Recovered	400
24.2.4	Voltage/Frequency Regulation and Power Sharing	400
24.3	Unexpected Problems Emerged During the Field Trial	402
24.4	Summary	404

<b>25</b>	<b>Texas Panhandle Wind Power System</b>	<b>405</b>
25.1	Geographical Description	405
25.2	System Structure	406
25.3	Main Challenges	407
25.4	Overview of Control Strategies Compared	407
25.4.1	VSM Control	408
25.4.2	DQ Control	410
25.5	Simulation Results	411
25.5.1	VSM Control	412
25.5.2	DQ Control	415
25.6	Summary and Conclusions	416
	<b>Bibliography</b>	<b>417</b>
	<b>Index</b>	<b>441</b>

## List of Figures

- Figure 1.1** Structure of the book. 4
- Figure 2.1** Examples of divisive opinions in a democratic society. (a) 2016 UK Brexit Referendum. (b) 2016 US presidential election. 14
- Figure 2.2** The sinusoid-locked loop (SLL) that explains the inherent synchronization mechanism of a synchronous machine. 17
- Figure 2.3** Estimated electricity consumption in the US. 18
- Figure 2.4** A two-port virtual synchronous machine (VSM). 19
- Figure 2.5** SYNDEM grid architecture based on the synchronization mechanism of synchronous machines (Zhong 2016b, 2017e). (a) Electrical system. (b) Overall system architecture highlighting the relationship between the electrical system and the ICT system, where the dashed arrow indicates that it may not exist. 20
- Figure 2.6** A SYNDEM home grid. 24
- Figure 2.7** A SYNDEM neighbourhood grid. 25
- Figure 2.8** A SYNDEM community grid. 26
- Figure 2.9** A SYNDEM district grid. 27
- Figure 2.10** A SYNDEM regional grid. 28
- Figure 2.11** The iceberg of power system challenges and solutions. 30
- Figure 2.12** The frequency regulation capability of a VSM connected the UK public grid. 32
- Figure 3.1** Illustrations of the imaginary operator and the ghost operator. (a) The imaginary operator applied to  $\cos \theta$  and  $\sin \theta$ . (b) The  $g$ -operator applied to  $\cos \theta$ . (c) The  $g$ -operator applied to  $\sin \theta$ . 38
- Figure 3.2** The system pair that consists of the original system and its ghost. (a) The original system  $Z$ . (b) The ghost system  $Z_g$ . 40
- Figure 3.3** Illustration of the ghost power theory. 47
- Figure 4.1** Structure of an idealized three-phase round-rotor synchronous generator with  $p = 1$ , modified from (Grainger and Stevenson 1994, figure 3.4). 52
- Figure 4.2** The power part of a synchronverter is a basic inverter. 55

- Figure 4.3** The electronic part of a synchronverter without control. 55
- Figure 4.4** The electronic part of a synchronverter with the function of frequency and voltage control, and real and active power regulation. 58
- Figure 4.5** Operation of a synchronverter under different grid frequencies (left column) and different load conditions (right column). 61
- Figure 4.6** Experimental setup with two synchronverters. (a) System structure. (b) System photo. 62
- Figure 4.7** Experimental results in the set mode: output currents with 2.25 kW real power. 63
- Figure 4.8** Experimental results in the set mode: output currents (left column) and the THD of phase-A current (right column) under different real powers. (a) 250 W. (b) 500 W. (c) 1000 W. (d) 1500 W. 64
- Figure 4.9** Experimental results in the droop mode: primary frequency response. 65
- Figure 4.10** Experimental results: the currents of the grid, VSG, and VSG2 under the parallel operation of VSG and VSG2 with a local resistive load. 65
- Figure 4.11** Real power  $P$  and reactive power  $Q$  during the change in the operation mode. 65
- Figure 4.12** Transient responses of the synchronverter. (a) Transfer from grid-connected mode to standalone mode. (b) Re-synchronization. (c) Transfer from standalone mode to grid-connected mode. 66
- Figure 5.1** Structure of an idealized three-phase round-rotor synchronous motor. 70
- Figure 5.2** The model of a synchronous motor. 72
- Figure 5.3** PWM rectifier treated as a virtual synchronous motor. 72
- Figure 5.4** Directly controlling the power of a rectifier. 73
- Figure 5.5** Controlling the DC-bus voltage of a rectifier. 74
- Figure 5.6** Simulation results when controlling the power. (a) Grid and internal frequencies. (b) DC-bus voltage. (c) Real power. (d) Reactive power. (e) Voltage  $v_a$  and current  $i_a$ . (f) Voltages  $v_a$  and  $e_a$ . 75
- Figure 5.7** Simulation results when controlling the DC-bus voltage. (a) Grid and internal frequencies. (b) DC-bus voltage. (c) Real power. (d) Reactive power. (e) Voltage  $v_a$  and current  $i_a$ . (f) Voltages  $v_a$  and  $e_a$ . 76
- Figure 5.8** Experimental results when controlling the power. (a) Grid and internal frequencies. (b) DC-bus voltage. (c) Real power. (d) Reactive power. (e) Voltage  $v_a$  and current  $i_a$ . (f) Voltages  $v_a$  and  $e_a$ . 78
- Figure 5.9** Experimental results when controlling the DC-bus voltage. (a) Grid and internal frequencies. (b) DC-bus voltage. (c) Real power. (d) Reactive power. (e) Voltage  $v_a$  and current  $i_a$ . (f) Voltages  $v_a$  and  $e_a$ . 79
- Figure 6.1** Integration of a PMSG wind turbine into the grid through back-to-back converters. 83
- Figure 6.2** Controller for the RSC. 84

- Figure 6.3** Controller for the GSC. 86
- Figure 6.4** Dynamic response of the GSC. (a) Full simulation process. (b) Voltage and current around the wind change. 88
- Figure 6.5** Dynamic response of the RSC. (a) Full simulation process. (b) Voltage and current around the wind change. 89
- Figure 6.6** Real-time simulation results with a grid fault appearing at  $t = 6$  s for 0.1 s. (a) When the grid voltage drops by 50%. (b) When the grid frequency drops by 1%. 90
- Figure 7.1** Conventional (DC) Ward Leonard drive system. 94
- Figure 7.2** AC Ward Leonard drive system. (a) Natural implementation. (b) Virtual implementation. 94
- Figure 7.3** Mathematical model of a synchronous generator. 95
- Figure 7.4** Control structure for an AC WLDS with a speed sensor. 96
- Figure 7.5** Control structure for an AC WLDS without a speed sensor. 99
- Figure 7.6** An experimental AC drive. 100
- Figure 7.7** Reversal from a high speed without a load. (a) Speed. (b) Torque of the generator. (c) Current. (d) Voltage. 101
- Figure 7.8** Reversal from a high speed with a load. (a) Speed. (b) Torque of the generator. (c) Current. (d) Voltage. 102
- Figure 7.9** Reversal from a low speed without a load. (a) Speed. (b) Torque of the generator. (c) Current. (d) Voltage. 103
- Figure 7.10** Reversal from a low speed with a load. (a) Speed. (b) Torque of the generator. (c) Current. (d) Voltage. 103
- Figure 7.11** Reversal at an extremely low speed without a load. (a) Speed. (b) Torque of the generator. (c) Current. (d) Voltage. 104
- Figure 7.12** Reversal from a high speed without a load (without a speed sensor). (a) Speed. (b) Torque of the generator. (c) Current. (d) Voltage. 105
- Figure 7.13** Reversal from a high speed with a load (without a speed sensor). (a) Speed. (b) Torque of the generator. (c) Current. (d) Voltage. 105
- Figure 8.1** Typical control structures for a grid-connected inverter. (a) When controlled as a voltage supply. (b) When controlled as a current supply. 108
- Figure 8.2** A compact controller that integrates synchronization and voltage/frequency regulation together for a grid-connected inverter. 109
- Figure 8.3** The per-phase model of an SG connected to an infinite bus. 110
- Figure 8.4** The controller for a self-synchronized synchronverter. 111
- Figure 8.5** Simulation results: under normal operation. (a) Frequencies  $f$  and  $f_g$ . (b) Frequency tracking error  $f - f_g$ . (c) Amplitude  $E$  of the generated voltage  $e$ . (d) Amplitude of  $v - v_g$ . (e) Real power. (f) Reactive power. 115
- Figure 8.6** Simulation results: connection to the grid. (a)  $v_b$  and  $v_{gb}$ . (b)  $v_b - v_{gb}$ . 116

- Figure 8.7** Comparison of the frequency responses of the self-synchronized synchronverter ( $f$ ) and the original synchronverter with a PLL ( $f$  with a PLL). 116
- Figure 8.8** Dynamic performance when the grid frequency increased by 0.1 Hz at 15 s (left column) and returned to normal at 30 s (right column). (a) Synchronverter frequency  $f$  and the grid frequency  $f_g$ . (b) Output current of phase  $a$ . (c) Output voltage of phase  $a$ . 117
- Figure 8.9** Simulation results under grid faults: when the frequency dropped by 1% (left column) and the voltage dropped by 50% (right column) at  $t = 36$  s for 0.1 s. (a) Synchronverter frequency  $f$  and the grid frequency  $f_g$ . (b) Output current of phase  $a$ . (c) Output voltage of phase  $a$ . 118
- Figure 8.10** Experimental results: when the grid frequency was lower (left column) and higher (right column) than 50 Hz. (a) Synchronverter frequency  $f$ . (b) Grid frequency  $f_g$  from a three-phase PLL for comparison. (c) Amplitude  $E$  of the generated voltage  $e$ . (d) Real power at the terminal. (e) Reactive power at the terminal. 120
- Figure 8.11** Experimental results of the original synchronverter: when the grid frequency was lower than 50 Hz (left column) and higher than 50 Hz (right column). (a) Synchronverter frequency. (b)  $P$  and  $Q$ . 122
- Figure 8.12** Voltages around the connection time: when the grid frequency was lower (left column) and higher (right column) than 50 Hz. (a)  $v_b$  and  $v_{gb}$ . (b)  $v_b - v_{gb}$ . 122
- Figure 9.1** Controlling the rectifier DC-bus voltage without a dedicated synchronization unit. 126
- Figure 9.2** Controlling the rectifier power without a dedicated synchronization unit. 128
- Figure 9.3** Simulation results when controlling the DC bus voltage. (a) Frequencies. (b) DC bus voltage. (c) Real power. (d) Reactive power. 129
- Figure 9.4** Grid voltage and control signal. (a) Uncontrolled mode. (b) PWM-controlled mode. 130
- Figure 9.5** Grid voltage and input current. (a) Uncontrolled mode. (b) When  $Q_{\text{ref}} = 0$  Var. 130
- Figure 9.6** Simulation results when controlling the real power. (a) Frequencies. (b) DC-bus voltage. (c) Real power. (d) Reactive power. 131
- Figure 9.7** Experiment results: controlling the DC-bus voltage. (a) Frequencies. (b) DC bus voltage. (c) Real power. (d) Reactive power. (e)  $v_a$  and  $i_a$  in the uncontrolled mode. (f)  $v_a$  and  $i_a$  in the PWM-controlled mode. 133
- Figure 9.8** Experiment results: controlling the power. (a) Grid and internal frequencies. (b) DC-bus voltage. (c) Real power. (d) Reactive power. (e)  $v_a$  and  $i_a$  in the uncontrolled mode. (f)  $v_a$  and  $i_a$  in the PWM-controlled mode. 134
- Figure 10.1** Typical configuration of a turbine-driven DFIG connected to the grid. 137

- Figure 10.2** A model of an ancient Chinese south-pointing chariot (WIKIpedia 2018). 138
- Figure 10.3** A differential gear that illustrates the mechanics of a DFIG, where the figure of the differential gear is modified from (Shetty 2013). 139
- Figure 10.4** The electromechanical model of a DFIG connected to the grid. 140
- Figure 10.5** Controller to operate the GSC as a GS-VSM. 141
- Figure 10.6** Controller to operate the RSC as a RS-VSG. 143
- Figure 10.7** Connection of the GS-VSM to the grid. 147
- Figure 10.8** Synchronization and connection of the RS-VSG to the grid. 148
- Figure 10.9** Operation of the DFIG-VSG. 149
- Figure 10.10** Experimental results of the DFIG-VSG during synchronization process. 151
- Figure 10.11** Experimental results during the normal operation of the DFIG-VSG. 152
- Figure 11.1** Three typical earthing networks in low-voltage systems. 157
- Figure 11.2** Generic equivalent circuit for analyzing leakage currents. 158
- Figure 11.3** Equivalent circuit for analyzing leakage current of a grid-tied converter with a common AC and DC ground. 159
- Figure 11.4** A conventional half-bridge inverter. (a) Topology. (b) Average circuit model. 160
- Figure 11.5** A transformerless PV inverter. (a) Topology. (b) Average circuit model. 162
- Figure 11.6** Controller for the neutral leg. 163
- Figure 11.7** Controller for the inverter leg. 164
- Figure 11.8** Real-time simulation results of the transformerless PV inverter in Figure 11.5. 166
- Figure 12.1** STATCOM connected to a power system. (a) Sketch of the connection. (b) Single-phase equivalent circuit. 171
- Figure 12.2** A typical two-axis control strategy for a PWM based STATCOM using a PLL. 173
- Figure 12.3** A synchronverter based STATCOM controller. 174
- Figure 12.4** Single-line diagram of the power system used in the simulations. 178
- Figure 12.5** Detailed model of the STATCOM used in the simulations. 178
- Figure 12.6** Connecting the STATCOM to the grid. (a)  $V_{dc}$ . (b)  $V_g$ . (c) Real power. (d) Reactive power. (e)  $\theta$  and  $\theta_g$ . (f)  $e$  and  $v_g$  (phase  $a$ ). 180
- Figure 12.7** Simulation results of the STATCOM operated in different modes. (a)  $V_{dc}$ . (b)  $V_g$ . (c) Real power. (d) Reactive power. (e)  $\theta$  and  $\theta_g$ . (f)  $\delta = \theta - \theta_g$ . 181
- Figure 12.8** Transition from inductive to capacitive reactive power when the mode was changed at  $t = 3.0$  s from the Q-mode to the V-mode. (a)  $V_{dc}$ . (b)  $V_g$ . (c) Real power. (d) Reactive power. (e)  $\theta$  and  $\theta_g$ . (f)  $v_{ga}$  and  $i_{ga}$ . 182

- Figure 12.9** Simulation results of the STATCOM operated with a changing grid frequency. (a)  $V_{dc}$ . (b)  $V_g$ . (c) Real power. (d) Reactive power. (e)  $\theta$  and  $\theta_g$ . (f) Grid frequency. 183
- Figure 12.10** Simulation results of the STATCOM operated with a changing grid voltage. (a)  $V_{dc}$ . (b)  $V_g$ . (c) Real power. (d) Reactive power. (e)  $\theta$  and  $\theta_g$ . (f)  $V_g$  without the STATCOM. 184
- Figure 12.11** Simulation results with a variable system strength. (a)  $V_{dc}$ . (b)  $V_g$ . (c) Real power. (d) Reactive power. (e)  $\theta$  and  $\theta_g$ . (f)  $V_g$  without the STATCOM. 185
- Figure 13.1** Per-phase diagram with the Kron-reduced network approach. 188
- Figure 13.2** Phase portraits of the controller. (a) The frequency dynamics. (b) The field-excitation current dynamics. 190
- Figure 13.3** The controller to achieve bounded frequency and voltage. 193
- Figure 13.4**  $E_+$  surface (upper) and  $E_-$  surface (lower) with respect to  $P_s$  and  $Q_s$ . 196
- Figure 13.5** Illustration of the areas characterized by  $E_+$  lines and  $E_-$  lines. 196
- Figure 13.6** Illustration of the area where a unique equilibrium exists. (a) When the grid voltage is at the rated value. (b) When the grid voltage is 5% lower than the rated value. (c) When the grid voltage is 5% higher than the rated value. 198
- Figure 13.7** Real-time simulation results comparing the original (SV) with the improved self-synchronized synchronverter (improved SV). (a) Real power  $P_s$  and reactive power  $Q_s$ . (b) Frequency  $f$  and field-excitation current ( $M_{tf}$ ). (c) Voltage  $E$  (normalized) and the amplitude  $V_c - V_g$ . 200
- Figure 13.8** Phase portraits of the controller states in real-time simulations. (a) The frequency dynamics. (b) The field-excitation current dynamics. 201
- Figure 14.1** The controller of the original synchronverter. 207
- Figure 14.2** Active power regulation in a conventional synchronverter after decoupling. (a) The whole active power channel. (b) The simplified active power channel. 208
- Figure 14.3** Properties of the active power loop of a conventional synchronverter with  $X^{pu} = 0.05$ ,  $\omega_n = 100\pi \text{ rad s}^{-1}$ , and  $\alpha = 0.5\%$ . (a) Closed-loop eigenvalues. (b) Phase margin. 209
- Figure 14.4** VSM with virtual inertia and virtual damping. 210
- Figure 14.5** The small-signal model of the active-power loop with a virtual inertia block  $H_v(s)$ . 211
- Figure 14.6** Implementations of a virtual damper. (a) Through impedance scaling with a voltage controller. (b) Through impedance insertion with a current controller. 212
- Figure 14.7** A VSM in a microgrid connected to a stiff grid. 216
- Figure 14.8** Normalized frequency response of a VSM with reconfigurable inertia and damping. 217

- Figure 14.9** Effect of the virtual damping ( $J_v = 0.2$  s). 217
- Figure 14.10** A microgrid with two VSMS. 217
- Figure 14.11** Two VSMS operated in parallel with  $J_{v1} = J_{v2} = 1$  s. 218
- Figure 14.12** Two VSMS operated in parallel with  $J_{v1} = 0.5$  s and  $J_{v2} = 1$  s. 219
- Figure 14.13** Simulation results under a ground fault with  $J_v = 0.1, 0.3, 0.5, 1$  s.  
(a) Normalized frequency. (b) Normalized fault current. 219
- Figure 14.14** Experimental results with reconfigurable inertia and damping.  
(a)  $J_v = 0.1$  s. (b)  $J_v = 1$  s. 220
- Figure 14.15** Experimental results from the original synchronverter for comparison. 221
- Figure 14.16** Experimental results showing the effect of the virtual damping with  $J_v = 0.2$  s. (a) Without virtual damping. (b) With virtual damping. 222
- Figure 14.17** Experimental results when two VSMS with the same inertia time constant are in parallel operation:  $J_{v1} = J_{v2} = 0.5$  s and  $\zeta_0 = 1$ . 223
- Figure 14.18** Experimental results when two VSMS with the same inertia time constant are in parallel operation:  $J_{v1} = J_{v2} = 1$  s and  $\zeta_0 = 0.707$ . 223
- Figure 14.19** Experimental results when two VSMS with different inertia time constants operated in parallel. 224
- Figure 14.20** Experimental results when the two VSMS operated as the original SV in parallel operation with  $\tau_{\omega1} = \tau_{\omega2} = 1$  s for comparison. 225
- Figure 15.1** Block diagrams of a conventional PLL. (a) Operational concept.  
(b) A simple PLL. 230
- Figure 15.2** Enhanced phase-locked loop (EPLL) or sinusoidal tracking algorithm (STA). 231
- Figure 15.3** Power delivery to a voltage source through an impedance. 232
- Figure 15.4** Conventional droop control scheme for an inductive impedance.  
(a) Without considering the integral effect. (b) With the hidden integral effect explicitly considered. 233
- Figure 15.5** Conventional droop control strategies. (a) For resistive impedance. (b) For inductive impedance. (c) For capacitive impedance. 234
- Figure 15.6** Linking the droop controller in Figure 15.4(b) and the (inductive) impedance. 235
- Figure 15.7** Droop control strategies in the form of a phase-locked loop. (a) When the impedance is inductive. (b) When the impedance is resistive. 237
- Figure 15.8** The conventional droop controller shown in Figure 15.4(a) after adding two integrators and a virtual impedance. 238
- Figure 15.9** The synchronization capability of the droop controller shown in Figure 15.8. (a) When  $v_g$  crosses 0. (b) When  $v_g$  is at the peak value  $V_g$ . 240
- Figure 15.10** Connection of the droop controlled inverter to the grid. 241
- Figure 15.11** Regulation of the grid frequency and voltage in the droop mode. 241

- Figure 15.12** Robustness of synchronization against DC-bus voltage changes. (a) When the DC-bus voltage  $V_{DC}$  was changed from 200 V to 180 V. (b) When the DC-bus voltage  $V_{DC}$  was changed from 180 V to 200 V. 242
- Figure 15.13** System response when the operation mode was changed. 243
- Figure 16.1** A single-phase inverter. (a) Used for physical implementation. (b) Used for controller design. 246
- Figure 16.2** Controller to achieve a resistive output impedance. 247
- Figure 16.3** Controller to achieve a capacitive output impedance. 248
- Figure 16.4** Typical output impedances of L-, R-, and C-inverters. 249
- Figure 16.5** Two R-inverters operated in parallel. 249
- Figure 16.6** Conventional droop control scheme for R-inverters. 249
- Figure 16.7** Experimental results: two R-inverters in parallel with conventional droop control. (a) Real power. (b) Reactive power. (c) Load voltage. (d) Voltage set point. (e) Frequency. (f) Currents. 250
- Figure 16.8** Robust droop controller for R-inverters. 253
- Figure 16.9** Experimental results for the case with a linear load when inverters have different per-unit output impedance: with the robust droop controller (left column) and with the conventional droop controller (right column). (a) Reactive power. (b) Real power. (c) RMS value of the load voltage. (d) Voltage set point. (e) Frequency. (f) Current in the steady state. 256
- Figure 16.10** Experimental results for the case with a linear load when inverters have the same per-unit impedance: with the robust droop controller (left column) and with the conventional droop controller (right column). (a) Reactive power. (b) Real power. (c) RMS value of the load voltage. (d) Voltage set point. (e) Frequency. (f) Current in the steady state. 258
- Figure 16.11** Experimental results for the case with the same per-unit impedance using the robust droop controller: with  $K_e = 10$  (left column) and  $K_e = 1$  (right column). (a) Reactive power. (b) Real power. (c) RMS value of the load voltage. (d) Voltage set point. (e) Frequency. (f) Current in the steady state. 259
- Figure 16.12** Experimental results with a nonlinear load: with the robust droop controller (left column) and with the conventional droop controller (right column). (a) Voltage set point. (b) Real power. (c) Reactive power. (d) THD of the output voltage. (e) Output voltage in the steady state. (f) Currents in the steady state. 260
- Figure 16.13** Robust droop controller for C-inverters. 261
- Figure 16.14** Experimental results of C-inverters (left column) and R-inverters (right column) with a linear load  $R_L = 9 \Omega$ . (a) Real power. (b) Reactive power. (c) RMS output voltage. (d) THD of the output voltage. (e) Output voltage at the steady state. (f) Current at the steady state. 263
- Figure 16.15** Experimental results of C-inverters (left column) and R-inverters (right column) with a nonlinear load. (a) Real power. (b) Reactive power. (c) RMS output voltage. (d) THD of the output voltage. (e) Output voltage at the steady state. (f) Current at the steady state. 264

- Figure 16.16** Robust droop controller for L-inverters. 265
- Figure 16.17** Experimental results of L-inverters with a linear load: with the robust droop controller (left column) and the conventional droop controller (right column). (a) Voltage set point. (b) Real power. (c) Reactive power. (d) THD of the output voltage. (e) Output voltage in the steady state. (f) Currents in the steady state. 266
- Figure 16.18** Experimental results of L-inverters with a nonlinear load: with the robust droop controller (left column) and with the conventional droop controller (right column). (a) Voltage set point. (b) Real power. (c) Reactive power. (d) THD of the output voltage. (e) Output voltage in the steady state. (f) Currents in the steady state. 267
- Figure 17.1** The model of a single-phase inverter. 270
- Figure 17.2** The closed-loop system consisting of the power flow model of an inverter and a droop controller. 271
- Figure 17.3** Interpretation of transformation matrices  $T_L$  and  $T_C$ . (a)  $T_L$ . (b)  $T_C$ . 273
- Figure 17.4** Interpretation of the universal transformation matrix  $T$ . 275
- Figure 17.5** Universal droop controller. 276
- Figure 17.6** Real-time simulation results of three inverters with different types of output impedance operated in parallel. (a) Real power. (b) Reactive power. (c) Frequencies. (d) RMS output voltage. (e) Output voltage. (f) Inductor currents. 278
- Figure 17.7** Experimental set-up consisting of an L-inverter, an R-inverter, and a C-inverter. 279
- Figure 17.8** Experimental results with the universal droop controller. (a)  $P$  and  $Q$ . (b)  $V_o$  and  $f$ . (c)  $v_o$  and  $i$ . 280
- Figure 18.1** The self-synchronized universal droop controller. 284
- Figure 18.2** Experimental results of self-synchronization with the R-inverter. (a) When started at  $v_g = 0$ . (b) When started at  $v_g = V_g$ . 288
- Figure 18.3** Experimental results when connecting the R-inverter to the grid. 289
- Figure 18.4** Experimental results with the R-inverter: performance during the whole experimental process. 289
- Figure 18.5** Experimental results with the R-inverter: regulation of system frequency and voltage in the droop mode. 290
- Figure 18.6** Experimental results with the R-inverter: change in the DC-bus voltage  $V_{DC}$ . (a) From 200 V to 180 V. (b) From 180 V to 200 V. 291
- Figure 18.7** Experimental results of self-synchronization with the L-inverter. (a) When started at  $v_g = 0$ . (b) When started at  $v_g = V_g$ . 292
- Figure 18.8** Experimental results with the L-inverter: connection to the grid. 292
- Figure 18.9** Experimental results with the L-inverter: performance during the whole experimental process. 293
- Figure 18.10** Experimental results with the L-inverter: regulation of system frequency and voltage in the droop mode. 293

- Figure 18.11** Experimental results with the L-inverter: change in the DC-bus voltage  $V_{DC}$ . (a) From 200 V to 180 V. (b) From 180 V to 200 V. 294
- Figure 18.12** Experimental results of self-synchronization with the L-inverter with the robust droop controller. (a) When started at  $v_g = 0$ . (b) When started at  $v_g = V_g$ . 295
- Figure 18.13** Experimental results from the L-inverter with the robust droop controller: connection to the grid. 296
- Figure 18.14** Experimental results from the L-inverter with the robust droop controller: performance during the whole experimental process. 296
- Figure 18.15** Experimental results from the L-inverter with the robust droop controller: regulation of system frequency and voltage in the droop mode. 297
- Figure 18.16** Experimental results with the L-inverter under robust droop control: change in the DC-bus voltage  $V_{DC}$ . (a) From 200 V to 180 V. (b) From 180 V to 200 V. 297
- Figure 18.17** A microgrid including three inverters connected to a weak grid. 298
- Figure 18.18** Real-time simulation results from the microgrid. (a) Real power and RMS voltage. (b) Reactive power and frequency. 299
- Figure 19.1** A general three-port converter with an AC port, a DC port, and a storage port. 303
- Figure 19.2** DC-bus voltage controller to generate the real power reference. 303
- Figure 19.3** The universal droop controller when the positive direction of the current is taken as flowing into the converter. 304
- Figure 19.4** Finite state machine of the droop-controlled rectifier. 306
- Figure 19.5** Illustration of the operation of the droop-controlled rectifier. 307
- Figure 19.6** The  $\theta$ -converter. 309
- Figure 19.7** Control structure for the droop-controlled rectifier. (a) Controller for the neutral leg. (b) Controller for the conversion leg. 310
- Figure 19.8** Experimental results in the GS mode. (a) Real power  $P$ , grid voltage  $V_g$ , reactive power  $Q$  and frequency  $f$ . (b) DC-bus voltage  $v_{DC}$ , DC-port voltage  $V_+$ ,  $P_{set}$  and  $K_{DC}$ . 313
- Figure 19.9** Experimental results in the NS-H mode. (a) Real power  $P$ , grid voltage  $V_g$ , reactive power  $Q$  and frequency  $f$ . (b) DC-bus voltage  $v_{DC}$ , DC-port voltage  $V_+$ ,  $P_{set}$  and  $K_{DC}$ . 314
- Figure 19.10** Experimental results in the NS-L mode. (a) Real power  $P$ , grid voltage  $V_g$ , reactive power  $Q$  and frequency  $f$ . (b) DC-bus voltage  $v_{DC}$ , DC-port voltage  $V_+$ ,  $P_{set}$  and  $K_{DC}$ . 315
- Figure 19.11** Transient response when the system starts up. (a) Real power  $P$ , grid voltage  $V_g$ , reactive power  $Q$  and frequency  $f$ . (b) DC-bus voltage  $v_{DC}$ , DC-port voltage  $V_+$ ,  $P_{set}$  and  $K_{DC}$ . 316
- Figure 19.12** Transient response when a load is connected to the system. (a) Real power  $P$ , grid voltage  $V_g$ , reactive power  $Q$  and frequency  $f$ . (b) DC-bus voltage  $v_{DC}$ , DC-port voltage  $V_+$ ,  $P_{set}$  and  $K_{DC}$ . 317